Controls on the Global Distribution of Martian Landsliding

Kevin P. Roback[1], Bethany L. Ehlmann[1,2]

[1] – Division of Geological and Planetary Sciences, California Institute of Technology, Pasadena, CA, USA

[2] – Jet Propulsion Laboratory, California Institute of Technology, Pasadena, California 91125, USA

Abstract

Recent acquisition of high-resolution satellite imagery of the Martian surface has permitted landsliding to be studied on a global scale on Mars for the first time. We apply the Scoops3D software package to compute slope stability for select regions of the Martian surface, combining calculations of slope stability with number of observed landslides, as reported in a recently published (Crosta et al., 2018a, b) inventory of Martian landslides, to understand controls on the global distribution of landsliding on Mars. We find that the distribution of landsliding does not simply follow the distribution of unstable slopes. In particular, there is an increase in landsliding in the Tharsis Rise area, and especially in Valles Marineris and Noctis Labyrinthus, that is not explained by an abundance of unstable topography alone. We analyzed for but did not find a clear local lithologic or stratigraphic control on landslide occurrence from subsurface heterogeneities. Other possibilities to explain the increased occurrence of landslides in the Tharsis Rise include (1) regionally widespread Tharsis weak unit(s), such as from

interbedded ashes and lavas; (2) seismic activity related to the Tharsis Rise's geological activity, and (3) possible groundwater near Valles Marineris into the Amazonian. Given the apparently young ages of many landslide deposits in Valles Marineris (Quantin et al., 2004), continued modern day analysis of lithologies in Valles Marineris and observations of Martian seismicity may act to strengthen or rebut the first two hypotheses.

Introduction

Since the arrival of the Mariner 9 spacecraft, large-scale landsliding has been observed on Mars in the Valles Marineris canyon system (e.g., Sharp, 1973; Lucchitta, 1979). Past investigations have focused on the mobility, age, formation and emplacement mechanisms of these landslides (e. g., McEwen, 1989; Quantin et al., 2004; Watkins et al., 2020). More recently, the proliferation of high-resolution imagery of the Martian surface generated by the CTX camera (Malin et al., 2007) has enabled landsliding to be studied on a global scale. In particular, Crosta et al. (2018a,b) have characterized Martian landsliding at a global scale for the first time with a published inventory of mapped Martian landslides (Fig. 1).

An area's landslide susceptibility is influenced by numerous factors. Some of these, such as hillslope angle and length, are observable from orbit. Others, such as rock strength, the presence of groundwater, and the history of seismicity in an area, are difficult or impossible to observe or infer from orbit. The study of spatial distributions of landsliding can thus provide insight into these factors, if the different mechanisms which can trigger landsliding can be distinguished uniquely.

We use the new (Crosta et al., 2018a) global landslide inventory in concert with global Martian datasets, including topography and faulting patterns, to undertake a comparative regional-scale analysis of factors driving the spatial distribution of landsliding on the Martian surface. We first investigate the hypothesis that the distribution of landsliding simply follows the distribution of unstable slopes on the Martian surface. We then consider the possible influence of spatially varying tectonic seismicity on Mars, the possible influence of variable rock strength, and the possible influence of groundwater on interpretation of our modeling results.

Methods

To quantify the relative susceptibility to landsliding of various topographies on Mars, we apply the Scoops3D software package developed by the USGS (Reid et al., 2015). Scoops3D calculates the forces driving and resisting motion on a large number of possible spherical trial landslide surfaces generated underneath an input digital elevation model. The model splits a trial failure mass into columns, over each of which driving and resisting forces are calculated and summed to derive an estimate of the ratio between the total forces resisting motion divided by the total forces driving motion of the trial landslide, known as the factor safety (FOS) (Fig. 2). Higher values of the FOS indicate greater stability. Unlike simpler slope stability modeling techniques, which are commonly based on applying 1D infinite-slope modeling techniques to individual cells of a DEM on a pixel-by-pixel basis, Scoops3D simulates trial landslide failure surfaces in 3D, integrating the effects of topographic

69 wavelength on the calculation of the stability of trial landslide surfaces, and the
70 determination of the most-probable landslide size.
71 For our analysis, we input elevation data from High Resolution Stereo
72 Camera (HRSC) DEMs, downsampled to a common resolution of 200m/pixel to
73 remove any potential influence of DEM resolution on the stability analysis. We chose
74 this HRSC DEM dataset because of its availability, its large regional coverage, and its
75 demonstrated greater accuracy in the steepest topography in comparison to CTX
76 DEMs created by us.
77 To calculate the FOS, we input into Scoops3D a constant set of material
78 parameters, including cohesion, angle of internal friction, and weight, for all study
79 areas to best isolate the impact of topography alone on the relative stability of
80 different Martian landscapes. Parameters were set to values corresponding to a low-
81 end rock strength. In particular, the cohesion was set to 1 MPa, the angle of internal
82 friction to 30 degrees, and the weight of material to 10 kN/m^3. Typical cohesions for
83 terrestrial rocks range from ~1-100 MPa; angles of internal friction can vary from
84 ~15 to 50 degrees (Goodman, 1980). Note that the weight of material is set lower
85 than typical weights of terrestrial rocks and soils (20-30 kN/m^3) due to Mars's
86 lower gravity (~38% of Earth's). The permissible volume range of trial landslide
87 failure surfaces was set to 10^8 – 10^{12} m^3; the high bound on possible landslide
88 volume is set given the scale of landslide deposits observed in Valles Marineris
89 (Lucchitta, 1979). A Bishop's simplified limit-equilibrium method was used. This
90 method assumes horizontal side forces, computed on the basis of the column's
91 weight and the angle of the sliding surface below the center of each column,

between the vertical columns comprising the modeled landslide failure mass. Earthquake loading and the presence of groundwater were not incorporated into the model setup.

The distribution of landsliding was then compared to the distribution of unstable slopes, i.e., slopes below a given factor of safety, via means of a window-based analysis. Analyzed parts of the Martian surface were divided into 20-km square windows. Within each window, the number of landslides was tallied, along with the fraction of the topography with a calculated factor-of-safety below a certain threshold deemed "unstable". We varied the threshold FOS to evaluate sensitivity to the choice, using values ranging from 3 to 6. In all plots presented here, we use 4 as the "unstable" threshold factor of safety value unless otherwise noted as the results were not very sensitive to the choice. The range of values we explored for the FOS threshold is informed partially by the range of FOS values computed for areas of observed, recent landsliding on Mars; a histogram of FOS values acquired in the vicinity of mapped Martian landslides is provided in Fig. 3. Over the range of considered threshold values, landsliding goes from being extremely abundant in topographies at FOS < 3 to extremely rare at FOS = 6. Of the ~2000 landslides that lie within areas covered by our FOS modeling, >95% occur in areas with a modeled FOS < 4, hence the choice of 4 as a threshold instability value. This pattern of FOS values holds whether we consider the FOS values computed at the centroid of the landslide's source area (Fig. 3., left panel), or the FOS values computed in a 5-km circular neighborhood around the centroid of the source area (Fig. 3, right panel).

Windows were then binned by their fractional percentage of unstable slopes, and landslide populations of bins with the same percentage of unstable slopes were compared across different geographic regions of the Martian surface. Studied and compared regions include Valles Marineris, Elysium Mons, Olympus Mons, Kasei Valles, Nili Fossae, Libya Montes, Noctis Labyrinthus, and a general region for all other studied terrain, which is mostly mapped as Noachian Highlands (Tanaka et al., 2014) (Fig. 4).

The statistical significance of differences in landslide occurrence between bins from different regions was evaluated via the use of a Wilcoxon rank-sum test on the population of windows within each bin. The Wilcoxon rank-sum test was chosen because the populations of landslides in each bin were generally distributed in a non-Gaussian way, with most windows hosting 0-1 landslides and a typically small number of windows hosting multiple landslides. If the output p-value from the rank-sum test was <0.05, indicating a >95% confidence that the difference in landsliding between the two bins was not a result of random sampling from the same distribution of landsliding, we consider the difference in landsliding between the bins to be statistically significant. Further, we only consider differences in landsliding to be significant if $p < 0.05$ is satisfied for different choices of the "unstable" threshold factor of safety value.

The Wilcoxon rank sum test often, but not always, supports statistically significant differences between pairs of bins in which the average number of landslides per window is greatly different. Reasons which can lead to $p > 0.05$ for such pairs of bins include small populations of windows in one or both bins as well

137 as the presence of outlier windows, e.g., when the number of windows in a one of
138 the pairwise compared bins is very small (generally <5) while there exists one or a
139 small number of windows with many (generally >5) landslides. These outlier
140 windows can significantly increase the average landsliding in a particular bin but
141 have less of an impact on the Wilcoxon rank sum test, which is more sensitive to the
142 overall comparison of distribution of landsliding across many windows.
143 In the analyses presented here, we group Martian terrain into 10 stability
144 bins, corresponding to 10% increments of unstable slope abundance. In general,
145 decreasing the number of bins acts to increase the number of windows in each bin,
146 increasing the odds of differences being found statistically significant. However,
147 larger bins group a greater range of terrains together, leaving more possibility for a
148 difference in landsliding between regions to be explainable as a difference in
149 topography. Sensitivity tests performed with different numbers of bins found that
150 our results were not generally sensitive to the number of bins used, for ranges of
151 ~5-20 bins.
152 To investigate the possible impact of tectonic seismicity on Martian
153 landsliding, we applied an inventory of surface faulting as mapped by Knapmeyer et
154 al., (2005). The previously described method of window-based analysis was
155 repeated, except that for the faulting case we compared populations of windows
156 that were within 50 km of a mapped Martian fault to populations of windows that
157 were more than 50 km from a mapped fault. Extremely large (M8-9) earthquakes on
158 Earth can trigger landsliding more than 200 km from the epicenter, but for M6-8
159 earthquakes 50-100 km is a more typical distance to the furthest landslides (Keefer,

1984). The distance of 50 km was also chosen in part because increasing the buffer around faults beyond this distance greatly decreases the amount of available terrain that is classified as far from a fault, hindering the ability of our statistical test to identify significant differences.

Results

We observe that, in general, topography is a primary control on the distribution of Martian landsliding. As expected, windows with abundant unstable terrain are much more likely to host a landslide, but even terrains that are >90% unstable have landslides in only ~20-40% of the terrain area windows (Fig. 5). However, significant differences in landsliding not related to topography are observed between some regions of the Martian surface. In particular, regions around the Tharsis Rise show more landsliding than regions elsewhere on Mars, even when controlling for percentage unstable topography and utilizing different factors of safety (Fig. 6).

These differences are most pronounced in comparing Noctis Labyrinthus (Fig. 6A, 6C) and Valles Marineris (Fig. 6B, 6D) to Noachian terrains. Landsliding is more common in these two regions in the heart of Tharsis than other Martian regions, and comparison of most bins of similar topographies shows differences in landsliding that are significant at >95% confidence level. These differences persist across different choices of the threshold factor-of-safety value used to define "stable" and "unstable" terrain. In other regions around Tharsis, such as Olympus Mons (Fig. 6E) and Kasei Valles (Fig. 6F) areas, landsliding is more common relative to Noachian terrain, but the differences in landsliding do not meet our criteria for

183 statistical significance for most bins, in part due to the small sizes of these regions
184 and correspondingly small populations of topographic "windows" with few
185 landslides each. We also attempted to compare Olympus Mons to Elysium Mons, in
186 an effort to compare large volcanic edifices near and far from Tharsis. However,
187 there is a general lack of steep topography in the Elysium Mons area comparable to
188 the aureoles surrounding the Olympus Mons edifice, which are the origin of most of
189 Olympus's landslides. Thus, the only comparable bins between the two regions are
190 low-instability bins with very few landslides; these bins do not host statistically
191 different landsliding.

192 Comparisons between different parts of the Tharsis Rise area (Fig. 7)
193 generally do not reveal statistically significant differences in landsliding, although
194 landsliding is more common in Valles Marineris and Noctis Labyrinthus relative to
195 other Tharsis areas. Additionally, we compare the eastern and western parts of the
196 Valles Marineris region to see if a contrast in the composition of subsurface
197 materials exhumed by impact craters, which was reported by Quantin et al. (2012),
198 has any apparent impact on landsliding. There is no statistically significant variation
199 in landsliding frequency across this lithologic contrast (Fig. 7C).

200 Mapped faulting also does not appear to be a major control on mapped
201 landsliding (Fig. 8). A global comparison of mapped landsliding for areas within 50
202 km of a mapped surface-exposed fault versus areas further away shows variation
203 only in the most unstable terrain (Fig. 8A). However, the terrain driving this
204 variation turns out to be concentrated almost exclusively in the Valles Marineris and
205 Noctis Labyrinthus areas (Fig. 8B & 8C). When these areas are excluded no

206 significant differences associated with windows close to or far from faulting are
207 observed elsewhere across the planet. In Valles Marineris, areas with >90%
208 unstable terrain have statistically higher landslide occurrences if <50 km from a
209 mapped fault (Fig. 8C).

210 *Discussion*

211 *Global Landslide Prevalence*

212 Our results comparing landslide occurrence in terrains of equivalent
213 instability suggest that the abundance of landsliding in regions around the Tharsis
214 Rise, and particularly near Valles Marineris, is not solely related to the presence of
215 abundant steep topography in this area. Landsliding correlates with topographic
216 stability in Tharsis, but not in Noachian highlands terrain, for the values of the
217 "unstable" factor of safety threshold presented here. The cause of this lack of
218 correlation may be the fact that most Noachian Highlands landslides are hosted in
219 the walls of impact craters. The slopes of these impact craters are rather short in
220 length, meaning that they occupy rather limited portions of the 20km-sided
221 windows considered in our analysis; this provides a population of landscape
222 windows that can host landslides despite having comparatively small areal extents
223 of unstable slopes. Larger craters with longer hillslopes filling larger portions of our
224 20-km windows do not exist in heavily cratered Noachian terrain, because craters
225 above 3-8 km in diameter take on complex-crater morphologies (Pike, 1980) with
226 wall slope angles set by the spontaneous gravitational collapse of the bowl-shaped
227 "transient crater" during an impact event.

Large areas of unstable slopes in Noachian terrain are uncommon; the largest of these is found in the fretted terrain in Nilosyrtis Mensae, which contains few visible landslides. This region shows extensive exposures of hydrated minerals (Bandfield & Amador, 2016), implying a possible abundance of groundwater in its distant past, but also may have experienced extensive glacial modification (Levy et al., 2007) erasing traces of landslides which may have occurred in the region's early history.

Interestingly, the Aeolis Mensae region, a geomorphologically similar region with fretted terrain along the boundary of the Noachian highlands, contains far more landslides. However, unstable slopes are actually less abundant in our studied regions of Aeolis Mensae relative to Nilosyrtis Mensae (Fig. 9). Evidence of a watery past is abundant in Aeolis (DiBiase et al., 2013) and a later stage of glacial activity may have occurred there as well (Davila et al., 2013), so the causes of the differences between these two regions are unclear. The Elysium Mons volcanic edifice, looming to the north of Aeolis, is a tempting factor, but its outer edge is located ~500 km from landslide-affected regions in Aeolis Mensae. This is in excess of the distances over which landslides are observed to be seismically triggered on Earth, even by extremely large earthquakes (Keefer, 1984).

The main question arising from our work is the cause of the elevated landsliding in Valles Marineris, and the Tharsis Rise region more broadly. Additional factors we have considered include possible enhanced Tharsis Rise seismicity, the possible presence of a "weak layer" or layers low in the stratigraphy in the Valles

Marineris area, and a possible atypical abundance of groundwater in the vicinity of the Valles Marineris area.

Why does the Tharsis area have more landslides?

A possible role for seismicity?

Seismicity associated with the extensive tectonic and volcanic activity surrounding the Tharsis Rise area may be a key contributor to landsliding, as suggested previously in the literature (Quantin et al., 2004). Although, as previously discussed, landsliding does not follow patterns of mapped faulting in general across Mars, faults may have been much more active in the vicinity of the Tharsis Rise, as would be expected given the scale of the chasmae and volcanic edifices present there. Indeed, there is a statistically significant increase in landsliding in windows with the most unstable topography (>90%) when those windows are <50 km from a fault (Fig. 8) in the Valles Marineris region. Additionally, Tharsis may harbor other deep faults obscured by comparatively recent volcanic activity. If seismicity is indeed the cause of landsliding in Valles Marineris, it may persist and be observable into the present day given the apparently youthful age of many landslide deposits (Quantin et al., 2004). Seismic data from InSight or future network missions may yet fully map Martian global seismicity.

A role for heterogeneous subsurface lithologies?

Another idea that has been suggested in the literature (Montgomery et al., 2009) is a rheologically "weak layer" at depth as a possible facilitator of large-scale gravity spreading in the Tharsis area. Such a layer could be dictated by mineralogy, e.g., clay minerals (e.g., Watkins et al., 2015; 2020) or by the physical properties of

273 the rock, e.g., loosely consolidated sediments or pyroclastics (e.g., Bandfield et al.,
274 2013). We mapped source areas of landslides throughout the Valles Marineris and
275 Noctis Labyrinthus regions, searching for debris-free landslide scarps from which
276 the elevation of the bottom of the landslide failure plane could be estimated (e.g. Fig.
277 10, panel A). We mapped an area including 1,766 landslides mapped by Crosta et al.,
278 but could only find clear basal scarps for 109 (~6%) of these landslides. This in
279 large part reflects modes of failure in Valles Marineris; most landslides in the
280 canyon are rock avalanches found below steep cliffs which lack a clear source area
281 (e. g., Fig. 10, panel D); slump-type landslides with clear scarps are less common.
282 Additionally, for many slumps, especially larger ones, much of the landslide mass
283 has not evacuated the scarp area; this leaves the basal shear surface obscured (Fig.
284 10, panel C).
285 The 109 identified basal scarps are clustered at low elevations in Valles
286 Marineris (Fig. 11) and are found preferentially in the eastern part of the canyon
287 system. The preference for the eastern part of the canyon for this form of scarp is
288 interesting as Quantin et al., (2012) previously reported a change in subsurface
289 lithology from west to east. Most of the successfully identified basal scarps are
290 relatively small in size (~1 km^2 or less) and are located at or below the elevation
291 (about -2000 m) at which low-calcium pyroxene (LCP)-rich, massive light-toned
292 rocks are reported to typically occur (Quantin et al., 2012; Flahaut et al., 2012) in
293 eastern Valles Marineris. Relative to the distribution of topography in Valles
294 Marineris, landslides are moderately more abundant than expected between -2000
295 and -4000 m elevation. It may be that these LCP lithologies or their boundaries with

296 adjacent units are more conducive to the formation of rotational slumps of this
297 scale; these rock units are described as “massive” (Quantin et al., 2012; Flahaut et
298 al., 2012), implying a lack of strong jointing or layering observable from orbit.
299 Terrestrial studies have found that landsliding in strongly jointed or layered rocks is
300 much more likely to take other forms including rockfalls, topples and rock
301 avalanches (Guzzetti et al., 1996; Hermanns & Strecker, 1999). However, slumping,
302 especially translational slumping along a plane of weakness, is still possible. Smooth
303 rotational slumps can also still form if the scale of failure is much larger than the
304 scale of layering or jointing, as intact rock is fractured between moving planes of
305 weakness.

306 Despite this clustering of slumps at low elevations, the abundance of total
307 landsliding remains similar from the lower-elevation slopes of Valles Marineris to
308 Noctis Labyrinthus, where chasma walls host landsliding at elevations of 3000 –
309 7000 m, above the levels at which much landsliding is observed in Valles Marineris,
310 and above the levels of previously suggested weak layers in the stratigraphy. If
311 stratigraphy in the Tharsis area is assumed to be generally horizontal, this variation
312 in elevations of landsliding implies that landsliding is hosted in a variety of rock
313 units of different ages. Lower elevation outcrops in the Valles Marineris system have
314 been interpreted as outcrops of primitive Noachian crust (Quantin et al., 2012;
315 Flahaut et al., 2012), while lava flows associated with Tharsis are thought to
316 comprise the stratigraphy at higher elevations (Murchie et al., 2009). Additionally,
317 landsliding is similarly present across the differences in subsurface materials
318 exhumed by impacts, observed by Quantin et al. (2012). This prevalence of

landsliding is an argument against characteristics of any particular lithologic unit controlling landslide distribution, although the morphological expression of landsliding may vary depending on strength and homogeneity of the particular rock unit and lithologic heterogeneities at smaller scale than observable from orbit could still play a role in dictating the planes of failure.

The layer of heavy slump activity may invoke comparisons to the weak layer suggested to exist by Montgomery et al. (2008) in the lower portions of Valles Marineris's stratigraphy, and to the low thermal inertia, putative volcaniclastic material inferred to exist by Bandfield et al. (2013). It is possible that material in the higher elevations of the Valles Marineris stratigraphy is indeed more well lithified than the lower-elevation massive layers, but the effective material strength at large scales may be set by systems of joints and fractures formed naturally from post-eruption cooling of the lava flows often assumed to comprise the higher parts of Valles Marineris stratigraphy.

A role for groundwater?

Groundwater presence, perhaps episodically related to periodic glacier formation on Tharsis, predicted by climate models (Fastook et al., 2008), and volcanic activity, is another possible contributor to enhanced landsliding. Groundwater fills pore spaces in rock; this both makes a bulk volume of rock heavier and induces a pore pressure which reduces stress normal to the failure plane, but does not reduce the shear stress parallel to the failure plane, leading to easier failure of slopes. Numerous outcrops of aqueous minerals are found in the Valles Marineris region (e.g., Murchie et al., 2009; Ehlmann & Edwards, 2014), and

many of these outcrops are interpreted to be relatively young (Milliken et al., 2008; Weitz et al., 2013), implying that groundwater and surface water may have persisted in this area longer than in other regions of the Martian surface. Given the inferred young age of many Valles Marineris landslides (Quantin et al., 2004) these relatively young mineral deposits could advance a case for groundwater as a potentially important factor.

Conclusions

By applying a new global inventory of landsliding and slope-stability modeling techniques, we analyzed patterns of Martian landsliding while controlling for the stability of topographies across different Martian terrains. The results indicate an abundance of landsliding around the area of the Tharsis Rise, and particularly around the Valles Marineris area. The effect is not solely due to the abundant steep topography in these areas. We analyzed for but did not find a clear local lithologic or stratigraphic control on landslide occurrence from heterogeneities in the crust. Other possibilities to explain the increased occurrence of landslides in the Tharsis Rise include (1) regionally widespread Tharsis weak unit(s), such as from interbedded ashes and lavas; (2) seismic activity related to the Tharsis Rise's geological activity, and (3) possible groundwater near Valles Marineris into the Amazonian. Given the apparently young ages of many landslide deposits in Valles Marineris (Quantin et al., 2004), continued modern day analysis of lithologies in Valles Marineris and observations of Martian seismicity may act to strengthen or rebut the first two hypotheses.

Acknowledgements

We thank Giovanni Crosta and Paolo Frattini for both providing early access to their Martian landslide inventory prior to its publication, and providing early feedback and critique of this work. We also thank Martin Knapmeyer for providing us with access to his mapped inventory of Martian faults. We also thank Jay Dickson for help in compiling and processing the Mars datasets. Our dataset of slope-stability calculations generated for this work is publically archived at CaltechDATA; doi: 10.22002/D1.1617.

Figures

Fig. 1 – The global landslide inventory, in point form and derived from CTX imagery, used as the basis of this analysis, by Crosta et al. (2018a) atop a grayscale Mars Orbiter Laser Altimeter (MOLA) global topographic map. All features aside from those mapped as rock glaciers are shown and were considered.

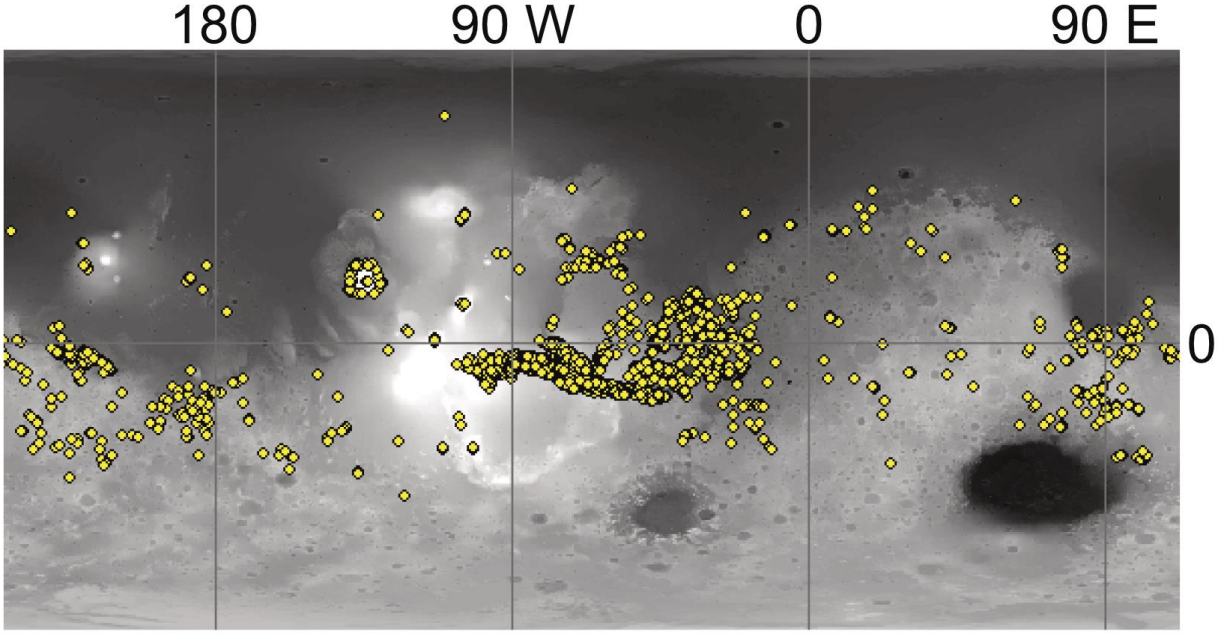

Fig. 2 – Simplified schematic of the rotational failure geometry and relevant forces as set up by the Scoops3D slope-stability model. W = column weight; N = normal force; S = shear force; R = distance from axis of rotation to base of a particular column in the trial failure mass.

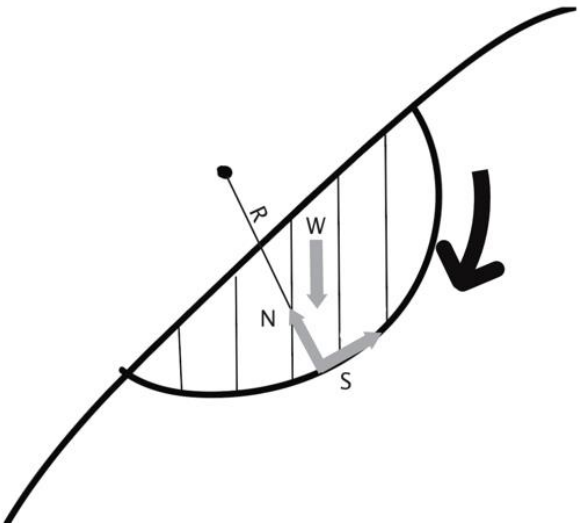

Fig. 3 – Left panel - FOS modeling results extracted at the centroids of source areas of landslides as mapped by Crosta et al. (2018). Right panel – FOS modeling results extracted across 5km circular windows around the centroids of mapped Martian landslides.

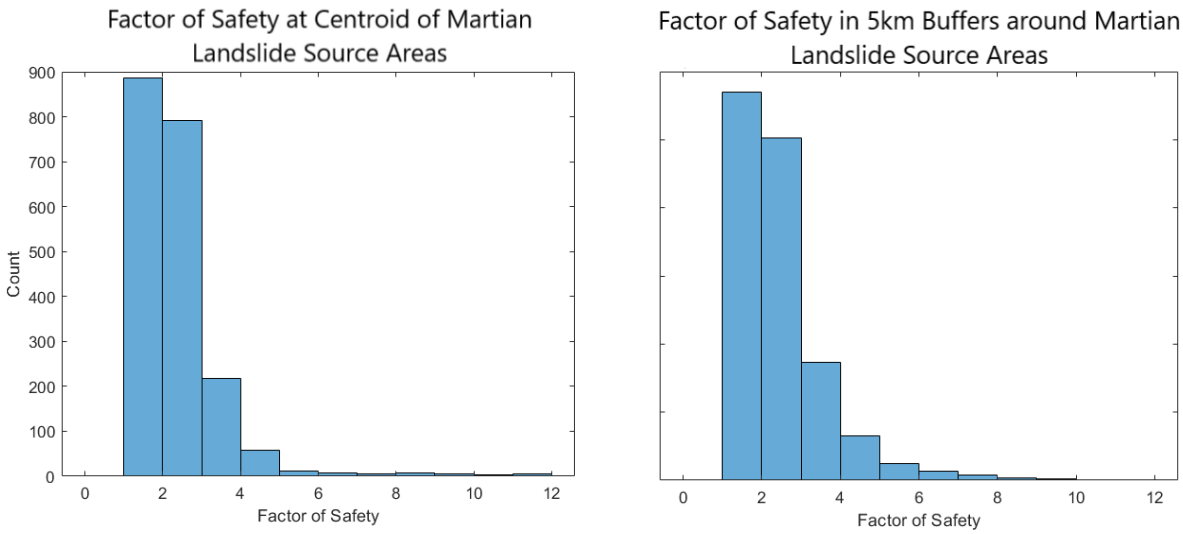

Fig. 4 – (A) – HRSC DEM coverage of the Scoops3D slope-stability modeling performed in this study atop MOLA topography. Regions of interest: EM = Elysium Mons; OM = Olympus Mons; NL = Noctis Labyrinthus; KV = Kasei Valles; VM = Valles Marineris; NH = Noachian Highlands; AM = Aeolis Mensae; NS = Nilosyrtis Mensae. (B) Scoops3D coverage for the Valles Marineris area. (C) Scoops3D coverage in areas near Syrtis Major.

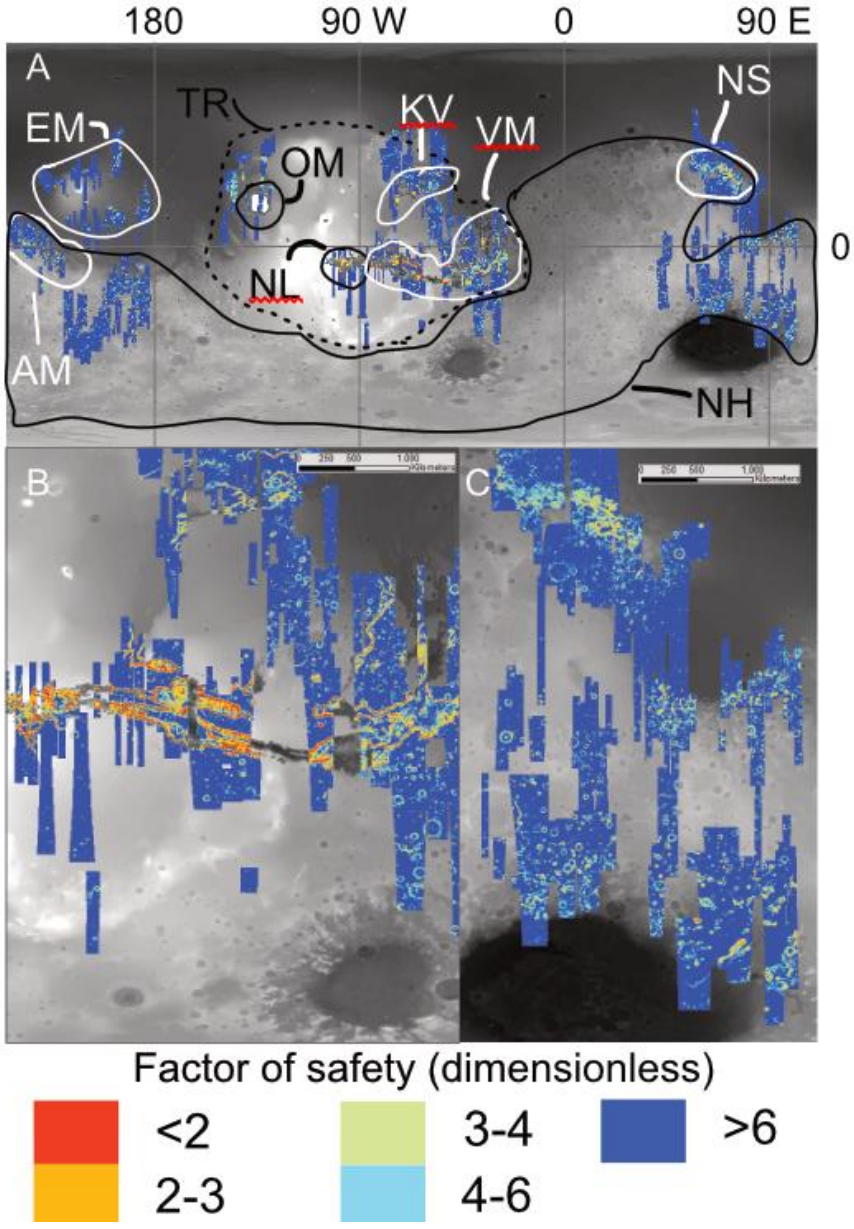

436 Fig. 5 – Abundance of landslides as a function of percent abundance of unstable
437 slopes, for all data averaged globally across the Martian surface. Gray line computed
438 using unstable FOS threshold = 3; black line using FOS threshold = 4 and gray
439 dashed line using FOS threshold = 6.

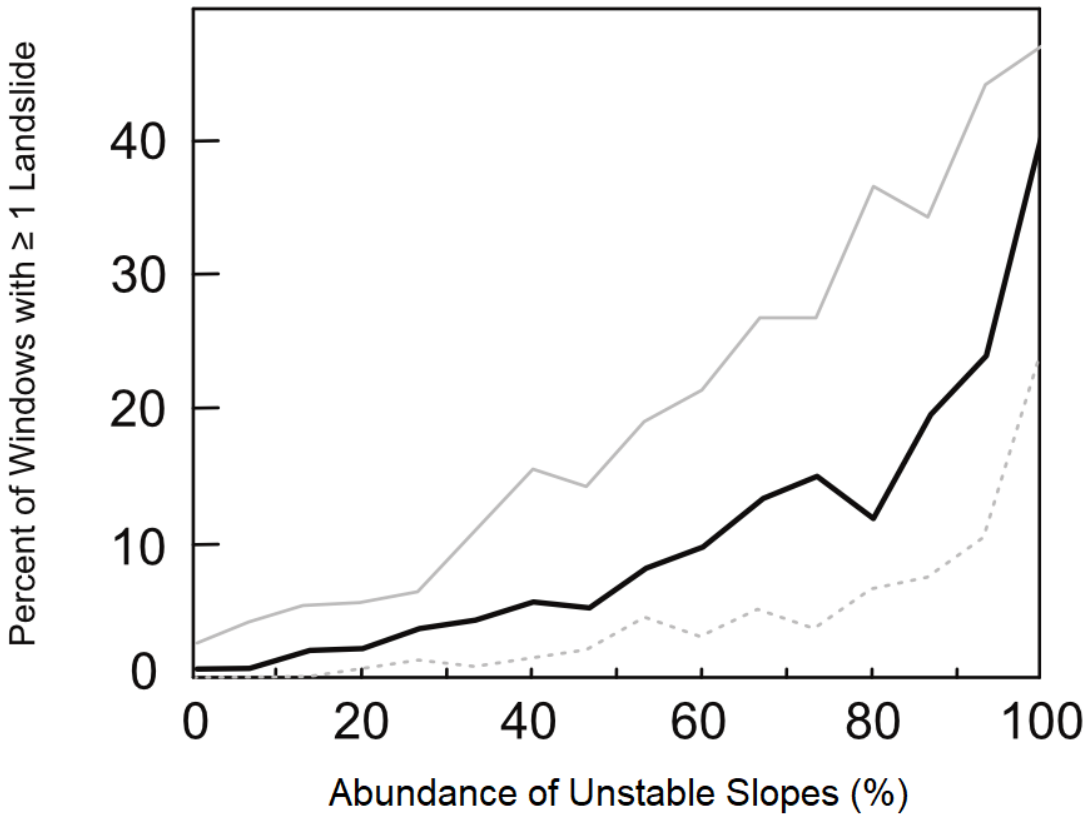

440
441
442
443
444
445
446
447

Fig. 6 – Comparisons of unstable slope vs landslide occurrence involving regions in the Tharsis Rise area, Noctis Labyrinthus (A, C) and Valles Marineris (B, D) as compared to Noachian Highlands terrain for different factors of safety. First row (A, B) indicates curves calculated using an unstable FOS threshold = 3; second row (C, D) indicates curves calculated using an unstable FOS threshold = 4. Areas in white are statistically significant while shaded areas mark parts of the curve in which the differences in landsliding between the compared regions are not significant at a 95% confidence level. In the lower panels, the solid lines correspond to the left y-axis and the dashed lines to the right y-axis.

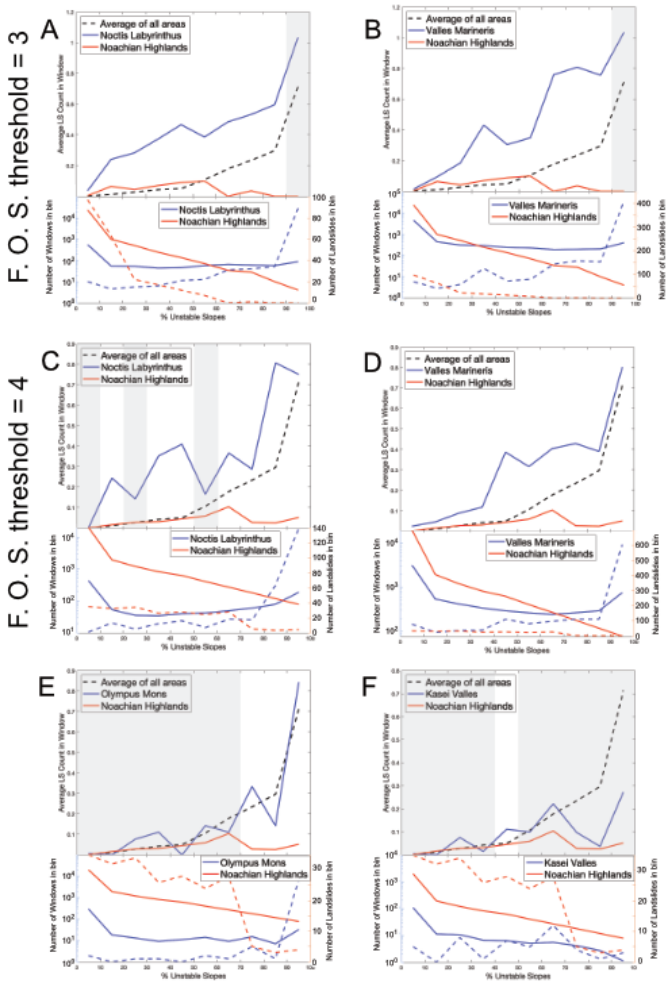

Fig. 7 – Comparisons of unstable slope vs landslide density between different regions in the vicinity of the Tharsis Rise; Olympus Mons & Valles Marineris (A), Kasei Valles & Valles Marineris (B), eastern and western Valles Marineris (C), and Noctis Labyrinthus and Valles Marineris (D & E). In panel C, the east/west division follows the contrast in subsurface material properties observed by Quantin et al., 2012. In panel D, an unstable FOS threshold of 3 is used to compute slope stability; in all other panels the unstable FOS threshold is assumed to be 4. Shading and axes correspondence to lines are as in Fig. 6.

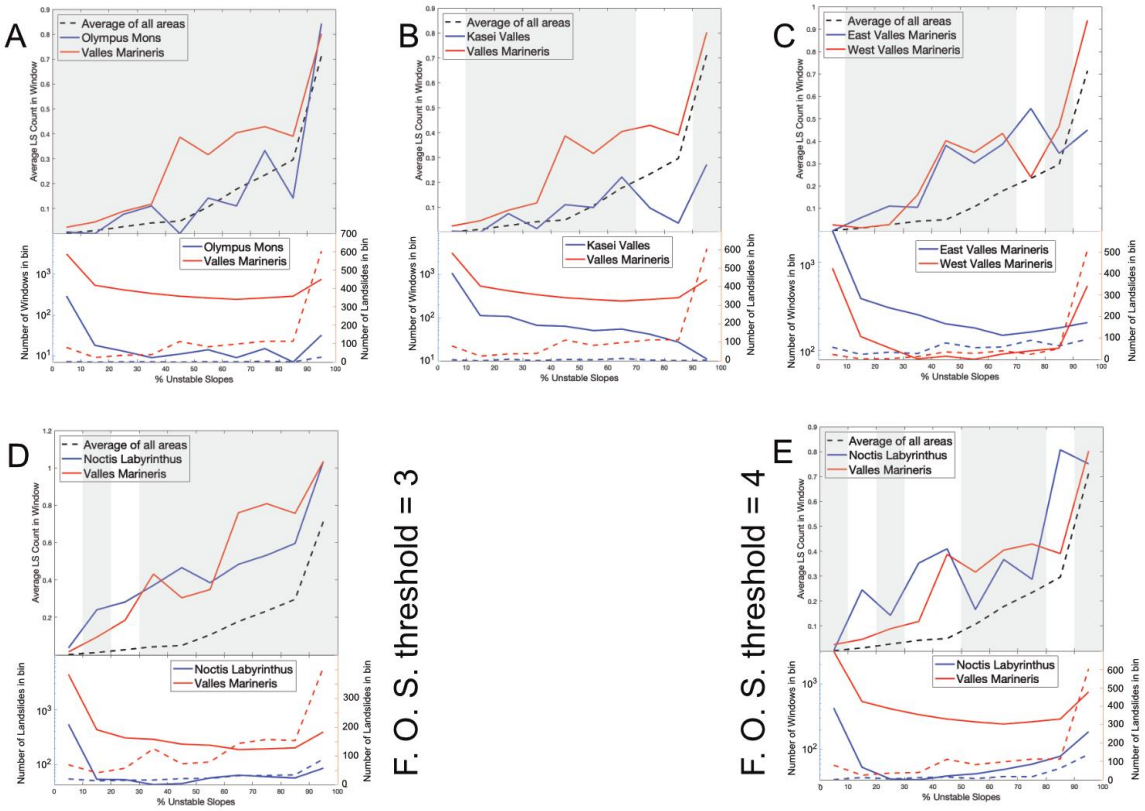

Fig. 8 – Comparison of landslide abundance as a function of slope stability for areas close to and far from a mapped fault, for all global data, for all global data excluding Valles Marineris, and for Valles Marineris only. Shading and axes correspondence to lines are as in Fig. 6.

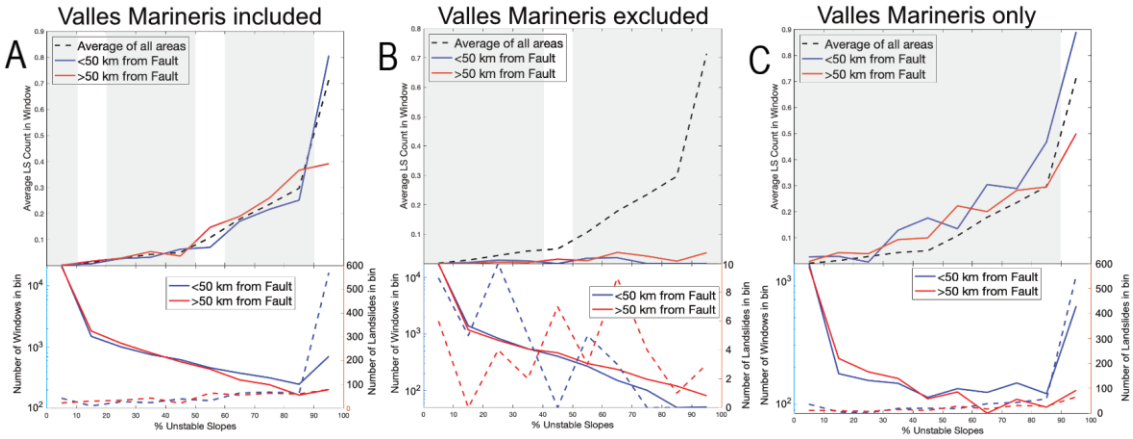

Fig. 9 – Comparison of abundance of unstable slopes for Nilosytis Mensae (blue bars) and Aeolis Mensae (red line).

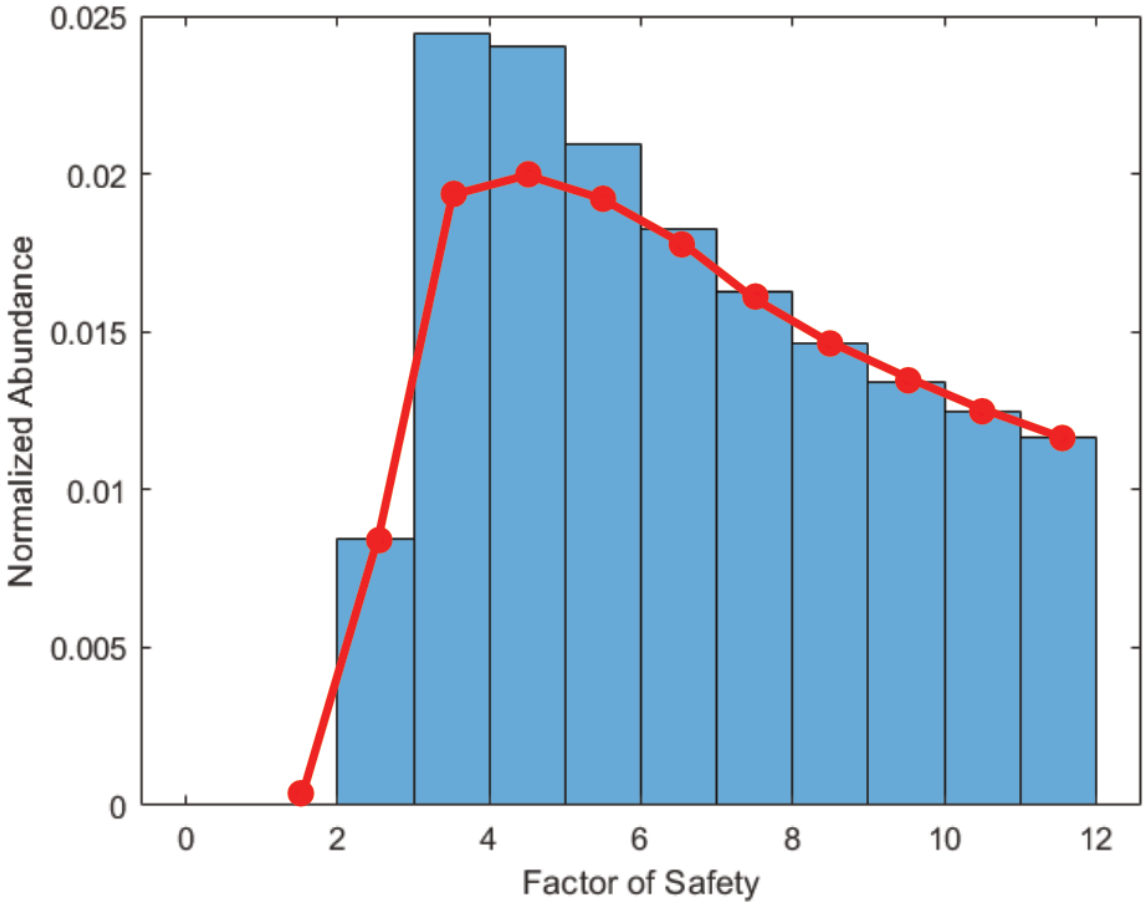

497 Fig. 10 – (A) and (B) Examples of landslides with an identifiable basal scarp in
498 eastern Valles Marineris. (C) Example of a large rotational slump whose scar is not
499 clear of landslide debris in Valles Marineris. (D) Area with several overlapping rock
500 avalanche deposits, but no clear corresponding source area on the cliffs above.

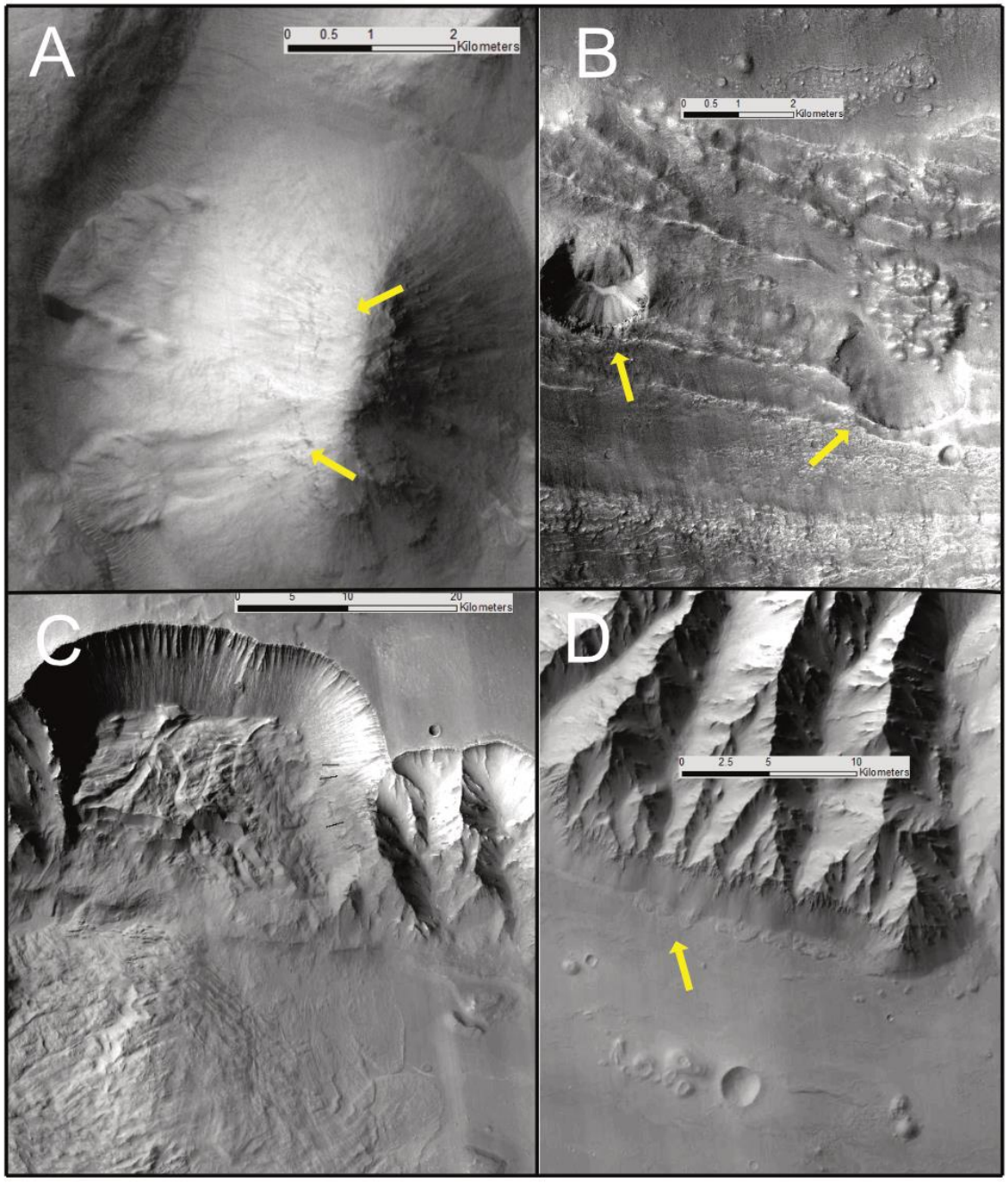

501

Fig. 11 – Blue line -Distribution of elevations of the bases of all mapped landslide scarps in Valles Marineris and Noctis Labyrinthus. Red bars – Distribution of elevation of slopes and canyon floor in the Valles Marineris study area. Inset – View of all mapped landslides in Valles Marineris (orange dots), and all landslides for which a scarp was successfully identified (yellow dots)

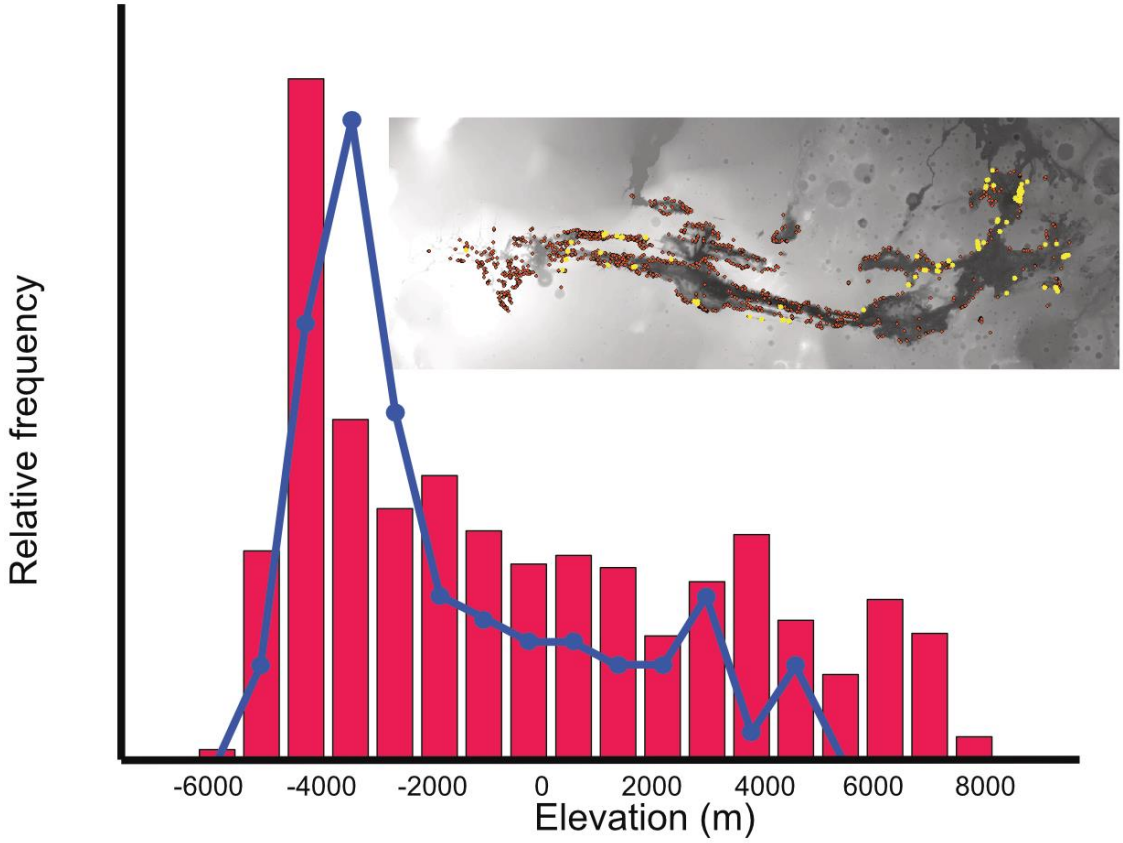

515 *References*

516 Bandfield, J. L., Edwards, C. S., Montgomery, D. R., & Brand, B. D., 2013, The dual
517 nature of the martian crust: Young lavas and old clastic materials: *Icarus*, v.
518 222, p. 188-199.
519 Bandfield, J. L. and Amador, E. S., 2016, Extensive aqueous deposits at the base of the
520 dichotomy boundary in Nilosyrtis Mensae, Mars: *Icarus*, v. 275, p. 29-44.
521 Crosta, G. B., Frattini, P., Valbuzzi, E., and De Blasio, F. V., 2018, Introducing a new
522 inventory of large Martian landslides: *Earth and Space Science*, v. 5, no. 4, p.
523 89-119.
524 Crosta, G. B., De Blasio, F. V., and Frattini, P., 2018, Global scale analysis of Martian
525 landslide mobility and paleoenvironmental clues: *Journal of Geophysical*
526 *Research: Planets*, v. 123, no. 4, p. 872-891.
527 Davila, A. F., Fairén, A. G., Stokes, C. R., Platz, T., Rodriguez, A. P., Lacelle, D., Dohm, J.,
528 and Pollard, W., 2013, Evidence for Hesperian glaciation along the Martian
529 dichotomy boundary: *Geology*, v. 41, no. 7, p. 755-758.
530 DiBiase, R. A., Limaye, A. B., Scheingross, J. S., Fischer, W. W., and Lamb, M. P., 2013,
531 Deltaic deposits at Aeolis Dorsa: Sedimentary evidence for a standing body of
532 water on the northern plains of Mars: *Journal of Geophysical Research:*
533 *Planets*, v. 118, no. 6, p. 1285-1302.
534 Ehlmann, B. L. & Edwards, C. S., 2014, Mineraology of the Martian surface:
535 *Annual Review of Earth & Planetary Sciences*, v. 42, p. 291-315.
536 Fastook, J. L., Head, J. W., Marchant, D. R., & Forget, F., 2008, Tropical mountain

glaciers on Mars: Altitude-dependence of ice accumulation, accumulation conditions, formation times, glacier dynamics, and implications for planetary spin-axis/orbital history: *Icarus*, v. 198, p. 305-317.

Flahaut, J., Quantin, C., Clenet, H., Allemand, P., Mustard, J. F., and Thomas, P., 2012, Pristine Noachian crust and key geologic transitions in the lower walls of Valles Marineris: Insights into early igneous processes on Mars: *Icarus*, v. 221, p. 420-435.

Goodman, R. E., 1980, Introduction to Rock Mechanics: *Wiley,* New York, 478 pp., 2nd ed.

Grotzinger, J. P., et al., 2014, A Habitable Fluvio-Lacustrine Environment at Yellowknife Bay, Gale Crater, Mars: *Science*, v. 343, no. 6169, 1242777.

Guzzetti, F., Cardinali, M., and Reichenbach, P., 1996, The Influence of Structural Setting and Lithology on Landslide Type and Pattern: *Environmental and Engineering Geoscience*, v. 2, no. 4, p. 531-555.

Hermanns, R. L., and Strecker, M. R., 1999, Structural and lithological controls on large Quaternary rock avalanches (sturzstroms) in arid northwestern Argentina: *GSA Bulletin*, v. 111, no. 6, p. 934-948.

Keefer, D. K., 1984, Landslides caused by earthquakes: *GSA Bulletin*, v. 95, p. 406-421.

Knapmeyer, M. E., Oberst, J., Hauber, E., Wählisch, M., Deuchler, C., and Wagner, R., 2006, Working models for spatial distribution and level of Mars' seismicity: *Journal of Geophysical Research: Planets*, v. 111, no. E11006, doi:10.1029/2006JE002708.

560 Levy, J. S., Head, J. W., and Marchant, D. R., 2007, Lineated valley fill and lobate
561 debris apron stratigraphy in Nilosyrtis Mensae, Mars: Evidence for phases of
562 glacial modification of the dichotomy boundary: *Journal of Geophysical*
563 *Research: Planets*, v. 112, no. E08004, doi:10.1029/2006JE002852.
564 Lucchitta, B. K., 1979, Landslides in Valles Marineris, Mars: *Journal of Geophysical*
565 *Research: Solid Earth*, v. 84, no. B14, p. 8097-8113.
566 Malin, M. C., et al., 2007, Context Camera Investigation on board the Mars
567 Reconnaissance Orbiter: *Journal of Geophysical Research: Planets*, v. 112, no.
568 E05S04, doi:10.1029/2006JE002808.
569 McEwen, A. S., 1989, Mobility of large rock avalanches: Evidence from Valles
570 Marineris, Mars: *Geology*, v. 17, p. 1111-1114.
571 Milliken, R. E., et al., 2008, Opaline silica in young deposits on Mars: *Geology*, v. 36,
572 no. 11, p. 847-850.
573 Montgomery, D. R., Som, S. M., Jackson, M. P. A., Charlotte Schreiber, B., Gillespie, A.
574 R., and Adams, J. B., 2009, Continental-scale salt tectonics on Mars and the
575 origin of Valles Marineris and associated outflow channels: *GSA Bulletin*, v.
576 121, no. 1-2, p. 117-133.
577 Murchie, S. L., et al., 2009, A synthesis of Martian aqueous mineralogy after 1 Mars
578 year of observations from the Mars Reconnaissance Orbiter: *Journal of*
579 *Geophysical Research: Planets*, v. 114, no. E00D06,
580 doi:10.1029/2009JE003342.
581 Quantin, C., Allemand, P., Mangold, N., and Delacourt, C., 2004, Ages of Valles

582 Marineris (Mars) landslides and implications for canyon history: *Icarus*, v.
583 172, p. 555-572.
584 Quantin, C., Flahaut, J., Clenet, H., Allemand, P., and Thomas, P., 2012, Composition
585 and structures of the subsurface in the vicinity of Valles Marineris as
586 revealed by central uplifts of impact craters: *Icarus*, v. 221, p. 436-452.
587 Reid, M. E., Christian, S. B., Brien, D. L., and Henderson, S. T., 2015, Scoops3D –
588 Software to Analyze Three-Dimensional Slope Stability Throughout a Digital
589 Landscape: U. S. Geological Survey Techniques and Methods, book 14, ch. A1,
590 218 p., doi:10.3133/tm14A1.
591 Sharp, R. P., 1973, Mars: Troughed Terrain: *Journal of Geophysical Research,* v. 78, no.
592 20, p. 4063-4072.
593 Tanaka, K. L., Robbins, S. J., Fortezzo, C. M., Skinner Jr, J. A., and Hare, T. M.,
594 2014, The digital global geologic map of Mars: Chronostratigraphic ages,
595 topographic and crater morphologic characteristics, and updated resurfacing
596 history: *Planetary and Space Science*, v. 95, p. 11-24.
597 Watkins, J. A., Ehlmann, B. L., and Yin, A., 2015, Long-runout landslides and the
598 lasting effects of early water activity on Mars: *Geology*, v. 43, no. 2, p. 107-
599 110.
600 Watkins, J.A., Ehlmann, B.L., Yin, A., 2020, 2020, Spatiotemporal evolution,
601 mineralogical composition, and transport mechanisms of long-runout
602 landslides in Valles Marineris, Mars: *Icarus*, 350, 113836.
603 Weitz, C. M., Bishop, J. L., & Grant, J. A., 2013, Gypsum, opal, and fluvial channels

within a trough of Noctis Labyrinthus, Mars: Implications for aqueous activity during the Late Hesperian to Amazonian: *Planetary and Space Science*, v. 87, p. 130-145.